THE JOURNAL OF PHYSICAL CHEMISTRY LETTERS
A JOURNAL OF THE AMERICAN CHEMICAL SOCIETY

pubs.acs.org/JPCL Letter

Formation of Methanol Clathrate Hydrate in Simulated Interstellar Ices

Soham Chowdhury, Bijesh K. Malla, Giridhar Baburao, Gopi Ragupathy,* and Thalappil Pradeep*

Cite This: https://doi.org/10.1021/acs.jpclett.6c01720 Read Online

ACCESS | Metrics & More | Article Recommendations | Supporting Information

ABSTRACT: We report that methanol, widely regarded as an inhibitor of clathrate hydrate (CH) formation, can be incorporated into a structure-I CH relevant to interstellar ices, under ultrahigh vacuum (10^{-10} mbar) and cryogenic (125 K) conditions. In the experiment, layered dimethyl ether (DME)−methanol−water ices were deposited at 10 K and thermally annealed to 125 K. Reflection−absorption infrared spectroscopy (RAIRS) reveals the emergence of a distinct band at 1021 cm^{-1} that is absent in pure CH_3OH and binary CH_3OH-H_2O ices. Density functional theory (DFT) calculations assign this band to the C−O stretching mode of methanol encapsulated in the $5^{12}6^2$ cage of structure-I CH. This clathrate occurs only in sequentially layered ices and requires a clathrate-promoting guest, such as DME. Similar behavior was observed with ethylene oxide, and methanol consistently occupies the $5^{12}6^2$ cage independent of the promoter molecule. RAIRS and DFT analyses further indicate that $CH_3OH\cdots H_2O$ hydrogen-bonded environments are involved in the methanol enclathration. These results identify a specific, morphology-dependent pathway through which methanol, traditionally considered a clathrate inhibitor, can be incorporated into the clathrate cages under nonequilibrium cryogenic conditions, with possible relevance to volatile trapping in thermally processed interstellar and cometary ices.

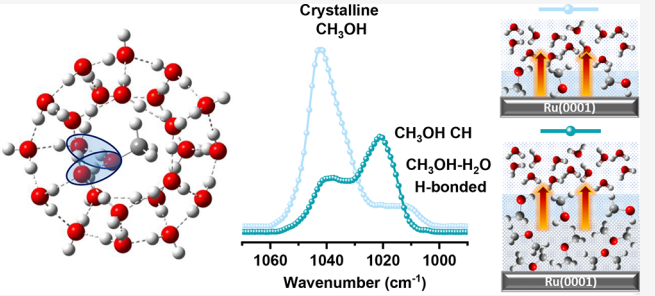

Methanol (CH_3OH) is one of the most abundant and chemically active molecules in the interstellar medium (ISM).[1,2] It forms efficiently on icy dust grains through the sequential hydrogenation of CO[3,4] and plays a central role in grain-surface chemistry by serving as a precursor to a wide range of oxygen-bearing organic molecules during thermal, UV, or electron-driven processing.[5−7] Upon desorption, methanol enriches the gas phase and participates in radical−radical and ion−molecule pathways, influencing the chemical evolution of dense clouds, protostellar environments, and cometary comae. Its prevalence and reactivity make methanol a key tracer of ice chemistry and thermal history in astrophysical environments.[3,8,9]

Beyond its astrochemical relevance, methanol also influences the physical and chemical properties of icy environments through its strong hydrogen-bonding interactions with water. Its volatility and antifreeze behavior modify the phase structure of mixed ices and affect the trapping and release of volatile species on icy bodies such as comets and outer Solar System objects.[10,11] In planetary atmospheres, trace amounts of methanol have been detected or inferred on Mars and Titan, where it may originate from photochemical oxidation of methane or from surface−atmosphere exchange processes. On earth, although present in only trace quantities, methanol plays a significant role in tropospheric oxidation chemistry, serving as both a source and a sink of hydroxyl (OH) radicals and influencing ozone formation and degradation cycles.

Clathrate hydrates (CHs), hydrogen-bonded water cages encasing guest molecules, represent a major condensed phase relevant to volatile trapping and release from icy planetary bodies, as well as during protostellar warming. Although CH formation is well documented for small apolar gases under high-pressure terrestrial conditions, the occurrence of clathrates under ultrahigh vacuum (UHV), analogous to the ISM, remains poorly understood. The extremely low mobility, structural disorder, and limited cage nucleation pathways in such ices present significant kinetic barriers, and only a few guest species have been shown to form CHs under UHV.[12−19] Demonstrating enclathration under these constraints is therefore essential for understanding volatile retention and segregation in interstellar and planetary ices far from equilibrium.

Methanol presents an additional complexity in this context. Despite its abundance in astrophysical ices, methanol is widely recognized as a thermodynamic inhibitor of CH formation on Earth, owing to its strong hydrogen bonding with water, which

Received: May 26, 2026
Revised: June 24, 2026
Accepted: June 26, 2026

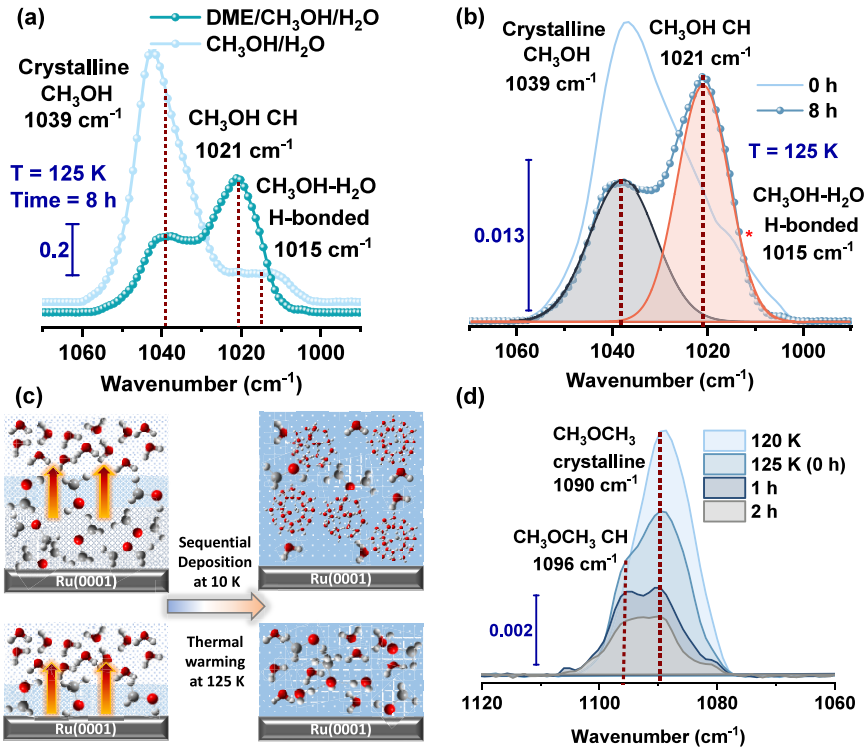

Figure 1. (a) Comparison of the RAIR spectrum of CH_3OH-H_2O ice (sky blue colored) and DME$-CH_3OH-H_2O$ ice (cyan colored) at 125 K after 8 h, respectively, in the methanol C−O stretching region. (b) Time-dependent RAIR spectra of DME$-CH_3OH-H_2O$ ice at 125 K. The spectrum at 8 h has been deconvoluted to quantify the fraction of CH formed. (c) Schematic diagram of the experimental protocol. (d) Temperature and time-dependent RAIR spectra of the C−O stretching of DME.

disrupts the cage-building network and stabilizes amorphous or solution-like phases.[20] Williams et al. reported the direct vapor deposition of mixed CH_3OH−ether CH at 115−130 K and Blake et al. reported diffraction evidence of methanol CH from methanol−water mixed ices upon heating from 85 to 130 K, both in high vacuum ($\sim 10^{-7}$ mbar).[21−23] However, Williams and Devlin subsequently argued that methanol is unlikely to form a clathrate under such conditions, as it preferentially crystallizes as the known monohydrate upon annealing of amorphous mixtures.[22] In high-pressure systems, methanol CH formation has also been observed in the presence of promoters or ionic solids.[20,24] Taken together, these observations suggest that methanol incorporation into clathrate cages typically requires either specific conditions or co-guests to overcome its inhibitory hydrogen-bonding interactions with water. Under UHV cryogenic conditions, direct spectroscopic evidence for methanol CH in amorphous methanol−water ices, and the mechanistic role of promoter guests in driving this process, have not been established. The present work addresses these aspects directly through RAIRS and DFT analysis of sequentially layered ices under UHV.

Here, we show that methanol can be incorporated into CH structures under UHV and cryogenic conditions relevant to interstellar ices. In contrast to its well-known inhibitory behavior, methanol becomes enclathrated when it is warmed up from amorphous ice in a sequentially layered dimethyl ether (DME)/CH_3OH/H_2O or ethylene oxide (ETO)/CH_3OH/H_2O configuration. Notably, methanol incorporation is not observed in pure CH_3OH ice, binary CH_3OH-H_2O ice, or any co-deposited DME$-CH_3OH-H_2O$ ice configurations, indicating that both a CH-forming co-guest and a layered ice morphology are essential for this process. Despite the presence of different promoters forming either sII (DME) or sI (ETO) CHs, methanol consistently occupies the $5^{12}6^2$ cage of an sI CH, suggesting a preferential stabilization of this configuration. These observations reveal that methanol enclathration is governed by a kinetically controlled mechanism involving molecular mobility, hydrogen-bonding interactions, and local ice structure. Together, these findings provide the first direct experimental evidence of methanol CH formation from amorphous ice under UHV cryogenic conditions and establish a new pathway for volatile trapping in astrochemically relevant environments.

All experiments were conducted using a custom-built ultrahigh vacuum (UHV) chamber, as described in detail in our previous study.[25] Thin ice films of CH_3OH, H_2O, and DME (or ETO) were prepared via background vapor deposition on a Ru(0001) single crystal. The ice thickness (in monolayers (ML)) was determined from the deposition time, background pressure and ionization gauge sensitivity factor. Quantum chemical calculations for both free and encapsulated CH_3OH and DME were performed using the B3LYP functional with the 6-311++G(d,p) basis set with the inclusion of Grimme's D3(BJ) dispersion correction. Additional methodological details are provided in the Supporting Information.

To probe the configurations enabling methanol enclathration under UHV cryogenic conditions, a series of pure, sequentially layered, and co-deposited ices were investigated using RAIRS. Although several control experiments, including pure CH_3OH and CH_3OH-H_2O ices, as well as co-deposited configurations with DME, did not yield any evidence of methanol CH formation, a distinctly different outcome emerged when DME (150 ML), methanol (50 ML), and

https://doi.org/10.1021/acs.jpclett.6c01720
J. Phys. Chem. Lett. XXXX, XXX, XXX−XXX

water (150 ML) were deposited as three separate layers (DME below CH_3OH, topped by H_2O) at 10 K and subsequently annealed to 125 K, as shown in Figure 1.

Analysis of the methanol C−O stretching region revealed a crucial difference. At 125 K, the initial spectrum (0 h) showed only crystalline CH_3OH (1039 cm^{-1}) and the $CH_3OH\cdots H_2O$ H-bonded complex centered near 1015 cm^{-1}. During isothermal annealing, however, a new band at 1021 cm^{-1} emerged, which grew progressively over time (Figure 1a,b). This feature was absent at the beginning of annealing and became clearly detectable after several hours.

In this arrangement, DME formed its characteristic CH feature at 1096 cm^{-1}.[15,26] The intensity of the 1096 cm^{-1} band decreased gradually over several hours (Figure 1d), indicating that the DME CH environment evolved over time as the methanol-related spectral changes developed.

To understand the origin of these spectral changes, we subsequently established the baseline behavior of methanol under UHV cryogenic conditions. We first examined the thermal evolution of pure CH_3OH and CH_3OH-H_2O ices. A 150 ML CH_3OH film deposited at 10 K was heated from 10 to 140 K. The reflection−absorption infrared (RAIR) spectra in Figure S2a exhibited the expected amorphous-to-crystalline phase transition; the broad amorphous C−O stretch at 1045 cm^{-1} sharpened into the phase-I (or phase α) crystalline methanol band at 90 K, followed by the emergence of the phase-II (or phase β) methanol feature at 1029 cm^{-1} above 110 K. Upon reaching the desorption temperature (∼140 K), CH_3OH desorbed substantially, leaving behind a minor residual phase-II crystalline component.[27,28]

Sequentially deposited CH_3OH/H_2O ices (50/150 ML total thickness) were studied under identical conditions. When heated to 125 K, the spectra showed crystalline methanol signatures at 1039 and 1029 cm^{-1} together with the characteristic methanol−water hydrogen-bonded complex at 1005−1020 cm^{-1} (Figure S2b). Dawes et al. and Müller et al. have reported similar spectral signatures for methanol−water mixed and layered ices.[29,30] These features also appeared in co-deposited CH_3OH-H_2O ices of 1:1 and 1:10 composition at elevated temperatures (Figure S2c,d). In all cases, crystalline methanol and $CH_3OH\cdots H_2O$ hydrogen-bonded complexes coexisted within the water matrix at elevated temperatures. Notably, no narrow peak or shoulder near 1021 cm^{-1} appeared in any CH_3OH-H_2O configuration (assigned below due to CH_3OH CH) at any temperature or composition, even during extended isothermal holds at 125 K.

Having established that methanol did not form CHs in either pure or CH_3OH-H_2O ices, we next examined whether the presence of a clathrate-forming guest molecule could promote methanol enclathration.[31−33] DME, a well-known CH-forming guest, was therefore introduced into the system (Figure S3).[15,26] Two configurations were investigated: (i) CH_3OH deposited below a co-deposited $DME-H_2O$ mixed ice and (ii) DME deposited below a co-deposited CH_3OH-H_2O layer at 10 K, followed by annealing to 125 K. In both cases, DME CH formation was observed through the appearance of the characteristic C−O stretching band at 1096 cm^{-1}. This feature has been previously assigned to the C−O stretching mode of DME encapsulated in CH cages.[15,26] Spectral deconvolution of this feature showed that the relative DME CH contribution was 52% for the co-deposited $DME-H_2O$ ice (Figure S3b), compared with 42% for the sequentially deposited DME/H_2O ice (Figure S1) and 39% for the $DME/CH_3OH/H_2O$ layered system (Figure S3d).

The comparatively larger DME CH fraction in the co-deposited $DME-H_2O$ ice is attributed to the intimate mixing of DME and H_2O prior to annealing, which facilitated clathrate formation. In contrast, in sequentially deposited DME/H_2O films, DME incorporation into hydrate cages competes with diffusion and desorption processes during annealing. The introduction of methanol further reduces the DME CH fraction, indicating that methanol perturbs DME clathrate formation. Consistent with this interpretation, the intensity of the 1096 cm^{-1} band decreased steadily and almost disappeared within 6 h at 125 K in methanol-containing systems. This behavior contrasted sharply with $DME-H_2O$ ices lacking methanol, where the DME CH was stable for more than 6 h under the identical conditions (Figure S1). These observations indicated that methanol inhibited the formation and stability of DME CH.[33−35] Consistently, the methanol spectral region displayed only crystalline CH_3OH bands and $CH_3OH\cdots H_2O$ H-bonded complexes, with no evidence of methanol CH formation in these mixtures.

Control experiments confirmed that the 1021 cm^{-1} feature did not arise from conventional methanol−water interactions. Temperature-dependent RAIRS of CH_3OH-H_2O mixtures with compositions of 1:1 and 1:10 exhibited only the broad 1005−1020 cm^{-1} envelope associated with $CH_3OH\cdots H_2O$ hydrogen-bonded complexes, consistent with prior IR and Raman studies. Importantly, no peak near 1021 cm^{-1} appeared in these systems at any temperature or annealing duration (Figure S2). Similarly, co-deposited $CH_3OH-DME$ ices capped with H_2O did not produce this feature (Figure S4), indicating that it did not arise from a direct $CH_3OH-DME$ interaction. The 1021 cm^{-1} band therefore emerged exclusively when a DME underlayer was present beneath the methanol and water films, as illustrated in the layered geometry of Figure 1c.

Additional evidence for the formation of CH was obtained from changes in the CH_3 rocking vibrational mode of CH_3OH.[27] The broad peak in the 1150−1110 cm^{-1} region gradually sharpened and evolved into a distinct feature at 1125 cm^{-1}, as the 1021 cm^{-1} band increased in intensity (Figure S6). Notably, the binary DME/H_2O spectra (Figure S1) show no feature in this region at any temperature or annealing duration, confirming that the observed evolution at 1125 cm^{-1} arises from methanol and not from DME spectral contributions. A similar spectral sharpening near 1125 cm^{-1} was reported by Williams et al. during the formation of sI and sII CH of CD_3OD, providing further support for assigning this feature to methanol enclathration.[22]

Taken together, these observations indicated that methanol did not form CH in CH_3OH-H_2O ices under UHV cryogenic conditions. However, when deposited in a layered configuration above a clathrate-forming guest such as DME, methanol was incorporated into the clathrate structure, producing a distinct and previously unobserved vibrational signature at 1021 cm^{-1}.

To identify the cage type responsible for the 1021 cm^{-1} feature, we carried out density functional theory (DFT) calculations and compared the computed C−O stretching frequencies of methanol in different clathrate cages with the experimental RAIRS data. Geometry optimizations were performed for isolated crystalline methanol and for methanol encapsulated within the three representative CH cages,

https://doi.org/10.1021/acs.jpclett.6c01720
J. Phys. Chem. Lett. XXXX, XXX, XXX−XXX

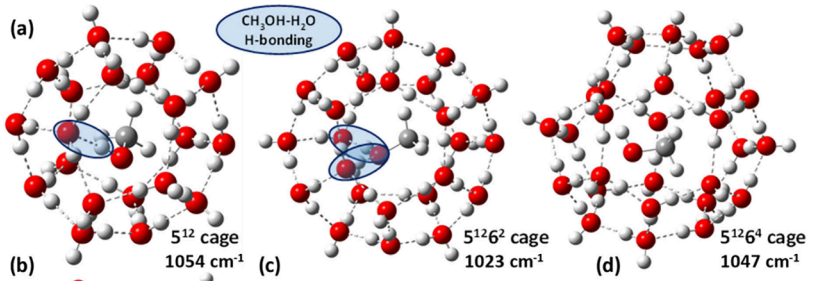

Molecule(s)	Experimental cm^{-1}	Theoretical cm^{-1}
CH_3OH	1039	1042
CH_3OH CH	1021 (-18)	1023 (-19)
CH_3OH-H_2O complex	1015	1013

CH_3OH	3.5 Angstroms
5^{12}	7.8 Angstroms
$5^{12}6^2$	8.6 Angstroms
$5^{12}6^4$	9.4 Angstroms

Figure 2. (a) DFT optimized CH structures of CH_3OH as 5^{12}, $5^{12}6^2$, and $5^{12}6^4$ cages. Blue ovals indicate the H-bonding between methanol and water. (b) DFT optimized H-bonded complexes of methanol and water. (c) Comparison of experimental and computational C−O stretching of methanol. (d) Comparison of the sizes of methanol and CH cages.

namely, 5^{12} (small), $5^{12}6^2$ (large cage of sI), and $5^{12}6^4$ (large cage of sII), as shown in Figure 2.[36] In all cases, methanol could be accommodated within the cage volume, consistent with the molecular dimensions relative to the cavity diameters.

The calculated C−O stretching frequency for crystalline methanol was 1042 cm^{-1}, in good agreement with the experimental band at 1039 cm^{-1} ($\Delta\upsilon$ = 3 cm^{-1}). Encapsulation of methanol within the three cage types resulted in distinct vibrational shifts. The $5^{12}6^2$ cage yielded a C−O stretching frequency of 1023 cm^{-1}, only 2 cm^{-1} higher than the experimentally observed band at 1021 cm^{-1}. In contrast, the 5^{12} and $5^{12}6^4$ cages produced C−O stretching frequencies at 1054 and 1047 cm^{-1}, respectively, which were significantly blue shifted relative to both crystalline methanol and the newly observed feature.

The magnitude and direction of the frequency shift further supported assignment to the $5^{12}6^2$ cage. Experimentally, the band associated with CH was red-shifted by 18 cm^{-1} compared to the crystalline methanol, whereas the DFT calculations predicted a red shift of 19 cm^{-1} for methanol confined within the $5^{12}6^2$ cage. In contrast, the 5^{12} and $5^{12}6^4$ cages exhibited blue shifts relative to the crystalline reference. This agreement between experiment and theory strongly supported assignment of the 1021 cm^{-1} band to methanol encapsulated in the $5^{12}6^2$ cage, characteristic of sI CH.

The optimized $5^{12}6^2$ structure provided a structural basis for this red shift. Two host−guest hydrogen bonds were formed, including one between the hydroxyl hydrogen of methanol and an oxygen atom of the water cage, and another between the methanol oxygen and a hydrogen of the cage water network. Participation of the methanol oxygen in hydrogen bonding weakened the C−O bond, accounting for the observed red shift in the C−O stretching frequency. In contrast, no comparable O···H hydrogen bond formed in the larger $5^{12}6^4$ cage, while the smaller 5^{12} cage restricted favorable alignment of the methanol oxygen, resulting in only a single hydrogen bond and a corresponding blue shift.

To further distinguish clathrate encapsulation from methanol−water hydrogen-bonded complexes, we modeled the representative $CH_3OH\cdots(H_2O)_n$ clusters (n = 1−3). Global-minimum structures and vibrational frequencies were computed to characterize the broad 1005−1020 cm^{-1} feature observed in CH_3OH−H_2O mixed ices. The calculations showed that one methanol coordinated with two water molecules (1:2 stoichiometry), in which the oxygen atom of CH_3OH accepted two hydrogen bonds, exhibited C−O stretches near 1013 cm^{-1}, consistent with the broad experimental feature centered around 1015 cm^{-1}. This assignment is in agreement with previous studies by Dawes et al., who attributed the broad feature near 1015 cm^{-1} to methanol molecules engaged in identical hydrogen-bonding interactions with water.[29] These values fell entirely within the broad complex band but clearly separated from the sharp 1021 cm^{-1} peak assigned to the clathrate formation.

The calculated stabilization energies further support the assignment. Methanol encapsulated in the $5^{12}6^2$ cage exhibited the most negative stabilization energy among the three cages (Table S1), indicating that this configuration was energetically favored. Together, the spectroscopic agreement and energetic preference confirmed that the newly observed 1021 cm^{-1} band corresponds to methanol encapsulated within the $5^{12}6^2$ cage of a CH formed under UHV cryogenic conditions.

To determine whether methanol CH formation was specific to DME or could be promoted by other small ethers, analogous RAIR experiments were performed using ETO as the underlying promoter layer (Figure S5). In the presence of ETO, the RAIR spectra displayed the characteristic 1021 cm^{-1} band associated with methanol encapsulated in the $5^{12}6^2$ cage, accompanied by ETO clathrate features at 1268 and 1275 cm^{-1}, consistent with sI ETO hydrate.[37] These results demonstrated that methanol enclathration was not unique to DME but could also occur in the presence of another small ether that is capable of forming hydrate cages.

The formation of methanol clathrate occurred only in the sequentially layered DME/CH_3OH/H_2O or ETO/CH_3OH/H_2O films and was absent in all co-deposited configurations. This contrast likely arose from differences in molecular interactions and mobility within amorphous cryogenic ices. In co-deposited DME−H_2O films, DME readily participated in cage formation upon annealing to 125 K, while methanol remained trapped as crystalline and $CH_3OH\cdots H_2O$ complexes. Similarly, in co-deposited CH_3OH−H_2O films, methanol rapidly formed hydrogen-bonded complexes with water and crystallized upon warming, thereby restricting its ability to

https://doi.org/10.1021/acs.jpclett.6c01720
J. Phys. Chem. Lett. XXXX, XXX, XXX−XXX

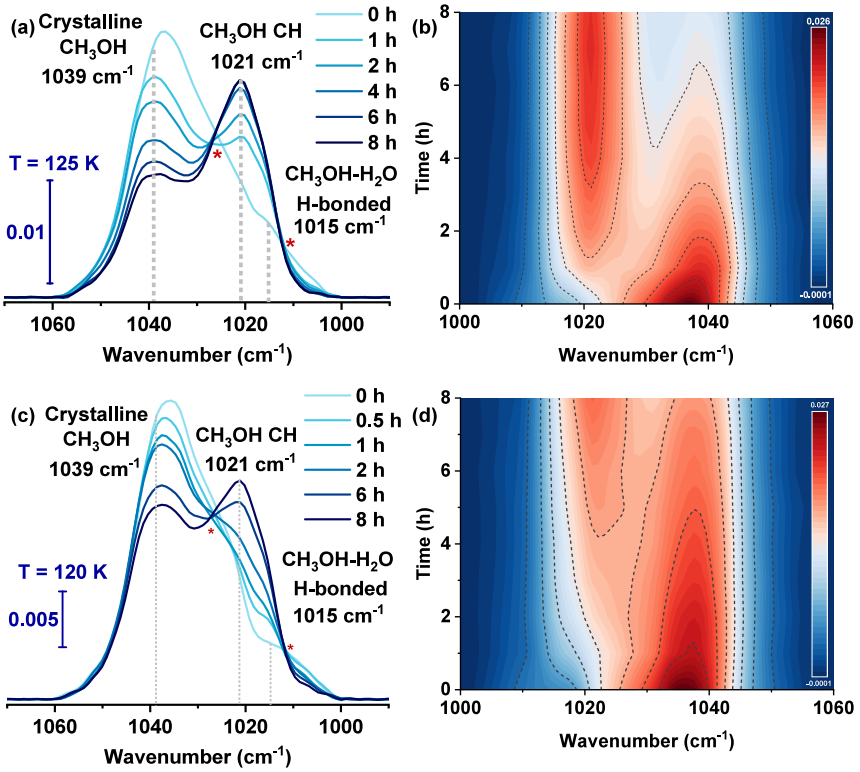

Figure 3. (a), (b) Time-dependent RAIR spectra of DME−CH_3OH−H_2O ice in CH_3OH C−O stretching region at 125 K. The isosbestic points were marked with *. (c), (d) Time-dependent RAIR spectra of DME−CH_3OH−H_2O ice in CH_3OH C−O stretching region at 120 K.

reorganize into cage-like motifs. Even when DME and CH_3OH were co-deposited, clathrate formation was not observed, possibly due to the higher mobility of the smaller CH_3OH molecule.

In contrast, the layered geometry initially isolated DME (or ETO), CH_3OH, and H_2O, minimizing the premature interactions. Upon annealing, both DME and methanol diffused toward the water matrix at comparable time scales. As DME nucleated sII cages, methanol likely remained sufficiently mobile to reorganize with the surrounding water network and occupy newly formed $5^{12}6^2$ cages. This sequence of events was kinetically inaccessible in fully mixed or precomplexed ices, highlighting the importance of sequential deposition for methanol enclathration.

The temporal evolution of the RAIR spectra during isothermal annealing (Figure 3) provided further insight into the transformation pathway leading to the formation of methanol CH. At 125 K, the C−O stretching region displayed two well-defined isosbestic points as the spectra evolved from 0 to 8 h. The presence of isosbestic points indicated that the spectral changes were dominated by interconversion among a limited number of species, consistent with three primary environments: crystalline methanol, $CH_3OH\cdots H_2O$ hydrogen-bonded complexes, and methanol incorporated into the CH cage.[38−40] In this scenario, the relative intensities of these species changed while the total concentration of absorbing oscillators remained conserved.

As the isothermal annealing proceeded, the intensity of the 1021 cm^{-1} CH band increased steadily, accompanied by a corresponding decrease in both the crystalline methanol features and the methanol−water complex band. The isosbestic behavior is consistent with $CH_3OH\cdots H_2O$ hydrogen-bonded complexes participating in the transformation pathway leading to clathrate nucleation, as partially solvated or hydrogen-bond-disordered methanol species possessed greater structural flexibility for incorporation into hydrate cages than molecules already arranged in the crystalline lattice. Given the spectral overlap and relatively low intensity of the complex band near 1015 cm^{-1}, the relative contributions of the crystalline and complex phases to this pathway cannot be quantitatively resolved from the present data.

A comparison of isothermal annealing at 120 and 125 K revealed a pronounced temperature dependence with clathrate formation being significantly more efficient at 125 K. This trend indicated that the increased molecular mobility of both methanol and DME within the water matrix facilitated the molecular rearrangements required for cage construction and guest encapsulation. Thus, the combined spectral kinetics and isosbestic behavior suggested a plausible transformation pathway in which methanol−water complexes reorganized at elevated temperature, enabling methanol to diffuse into emerging $5^{12}6^2$ cages and form the observed sI CH.

Additional experiments performed at 135 K revealed that methanol enclathration still occurs at higher temperature, as evidenced by the transient appearance of the 1021 cm^{-1} band (Figure S7). However, the CH feature decreases substantially within ∼30 min, accompanied by crystallization of the water matrix as observed in the O−H stretching region. These observations indicate that methanol CH becomes unstable at 135 K, placing its thermal stability limit between 120 and 135 K under the present UHV conditions. Thus, 125 K represents a near-optimal temperature at which molecular mobility is sufficient to promote cage formation while maintaining clathrate stability over extended annealing times.

To further probe the conditions under which methanol becomes incorporated into the clathrate structure, we

https://doi.org/10.1021/acs.jpclett.6c01720
J. Phys. Chem. Lett. XXXX, XXX, XXX−XXX

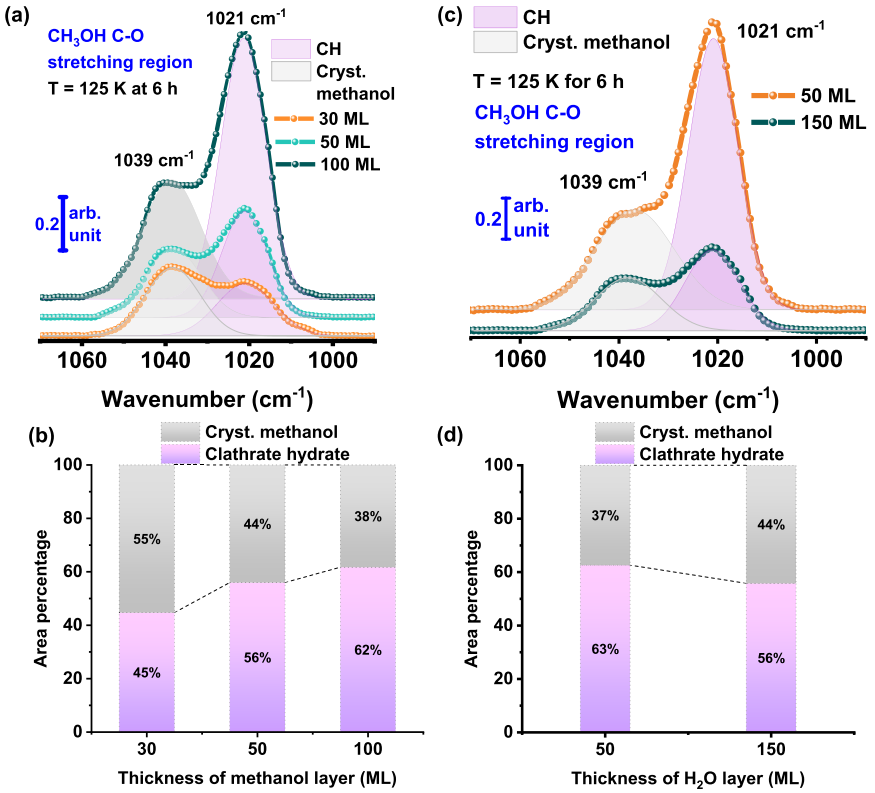

Figure 4. Thickness-dependent RAIR spectra in the C−O stretching region of CH_3OH and corresponding CH fraction from the deconvoluted spectra with increase in the thickness of (a), (b) CH_3OH and (c), (d) H_2O. CH fraction determined from the peak area of the 1021 cm^{-1} component.

examined the influence of the methanol and water film thickness on CH formation, keeping the DME underlayer fixed at 150 ML. Figure 4 summarizes the resulting trends after 6 h of isothermal annealing at 125 K. The relative fraction of methanol converted to CH, determined from the deconvoluted peak areas of the 1021 and 1039 cm^{-1} components, increased systematically with increasing methanol thickness, whereas increasing the amount of overlying water suppressed clathrate formation. We note that the absolute intensities of both the 1021 and 1039 cm^{-1} bands decreased with increasing water thickness; however, the relative population of methanol CH versus crystalline methanol, which is independent of this effect, showed a clear systematic trend with thickness.

These opposing dependencies could be rationalized in terms of desorption-assisted molecular mobility within the layered ice. At 125 K, both DME and CH_3OH underwent partial desorption, which increased molecular rearrangement and diffusion within the ice matrix.[41] When the methanol layer was thicker, the increased availability of mobile methanol molecules enhanced their ability to reorient and access emerging $5^{12}6^2$ cages, favoring clathrate incorporation over retention in crystalline or hydrogen-bonded environments. In contrast, thicker water overlayers inhibited methanol desorption and confined the molecules within stronger $CH_3OH\cdots H_2O$ hydrogen-bonded networks, thereby reducing the population of mobile methanol molecules available for cage entry. Notably, clathrate formation was not completely suppressed even at the highest water thickness tested, indicating a competition between mobility-driven enclathration and hydrogen-bonding confinement rather than complete inhibition.

These observations indicated that CH formation was highly sensitive to the balance between methanol mobility and hydrogen-bonding confinement within the ice. An optimal methanol-to-water ratio was therefore required to achieve sufficient molecular mobility for cage occupancy while avoiding the formation of strongly bound complexes that compete with CH nucleation.

In summary, we have shown that methanol can be incorporated into the $5^{12}6^2$ cage of sI CH under UHV and cryogenic conditions, despite being widely regarded as a clathrate inhibitor. This occurred only under specific conditions, particularly, the ices must be sequentially deposited, and a clathrate-promoting guest must be present. Co-deposited configurations consistently failed, because methanol formed hydrogen-bonded complexes with water before cage nucleation could begin. Time-dependent RAIRS revealed two isosbestic points linking crystalline methanol, $CH_3OH\cdots H_2O$ complexes, and the CH band, suggesting that hydrogen-bonded complexes participate in cage incorporation. Thickness-dependent experiments further showed that methanol mobility promotes clathrate formation, whereas stronger hydrogen-bonding environments suppress guest incorporation. At 135 K, methanol CH formation was also observed, but the structure dissociated within ∼30 min, accompanied by water ice crystallization, establishing an upper thermal stability boundary for this system.

These results showed that methanol's role in clathrate chemistry is not simply inhibitory; under the right morphological and kinetic conditions, it becomes a genuine CH guest. In astrochemical environments, the necessary prerequisites, compositionally distinct ice layers and thermally driven

https://doi.org/10.1021/acs.jpclett.6c01720
J. Phys. Chem. Lett. XXXX, XXX, XXX−XXX

molecular diffusion could be transiently realized during protostellar warm-up, where ice mantles accreted in distinct episodes undergo thermal restructuring and molecular segregation, or in cometary nuclei during episodic heating near perihelion. The present work therefore identifies a specific nonequilibrium pathway for methanol trapping in clathrate structures whose astrophysical relevance depends critically on local ice morphology and thermal history.

■ ASSOCIATED CONTENT

Supporting Information

The Supporting Information is available free of charge at https://pubs.acs.org/doi/10.1021/acs.jpclett.6c01720.

Experimental section (including experimental setup, materials and reagents, and sample preparation) and temperature- and time-dependent RAIR spectra, comparison of stabilization energies (PDF)

■ AUTHOR INFORMATION

Corresponding Authors

Gopi Ragupathy − *Department of Chemistry, School of Advanced Sciences, Vellore Institute of Technology, Vellore 632014, India;* orcid.org/0000-0002-9435-5712; Email: r.gopi@vit.ac.in

Thalappil Pradeep − *DST Unit of Nanoscience (DST UNS) and Thematic Unit of Excellence (TUE), Department of Chemistry, Indian Institute of Technology Madras, Chennai 600036, India; International Centre for Clean Water, IIT Madras Research Park, Chennai 600113, India;* orcid.org/0000-0003-3174-534X; Email: pradeep@iitm.ac.in

Authors

Soham Chowdhury − *DST Unit of Nanoscience (DST UNS) and Thematic Unit of Excellence (TUE), Department of Chemistry, Indian Institute of Technology Madras, Chennai 600036, India;* orcid.org/0009-0000-8151-6065

Bijesh K. Malla − *DST Unit of Nanoscience (DST UNS) and Thematic Unit of Excellence (TUE), Department of Chemistry, Indian Institute of Technology Madras, Chennai 600036, India;* orcid.org/0009-0005-1148-0884

Giridhar Baburao − *Department of Chemistry, School of Advanced Sciences, Vellore Institute of Technology, Vellore 632014, India*

Complete contact information is available at: https://pubs.acs.org/10.1021/acs.jpclett.6c01720

Author Contributions

S.C. designed and performed the experiments. S.C. and B.K.M. analyzed the results. T.P. supervised the work. G.B. and G.R. performed the quantum chemical calculations. The first draft of the manuscript was written by S.C. The final version of the manuscript was prepared, incorporating contributions from all authors.

Notes

The authors declare no competing financial interest.

■ ACKNOWLEDGMENTS

We acknowledge the Science and Engineering Research Board (SERB), Department of Science and Technology (DST), and Government of India for research funding. T.P. acknowledges support through a JC Bose Fellowship and funding from the Centre of Excellence on Molecular Materials and Functions under the Institution of Eminence scheme of IIT Madras. S.C. thanks IITM for his research fellowship. G.B. acknowledges the VIT Vellore for providing financial support through the institutional research fellowship. G.R. expresses gratitude to the management of VIT Vellore for providing access to sophisticated computational facilities.

■ REFERENCES

(1) Walsh, C.; Loomis, R. A.; Öberg, K. I.; Kama, M.; van't Hoff, M. L. R.; Millar, T. J.; Aikawa, Y.; Herbst, E.; Weaver, S. L. W.; Nomura, H. First Detection of Gas-Phase Methanol in a Protoplanetary Disk. *Astrophys. J. Lett.* **2016**, *823* (1), L10.

(2) Goto, M.; Vasyunin, A. I.; Giuliano, B. M.; Jiménez-Serra, I.; Caselli, P.; Román-Zúñiga, C. G.; Alves, J. Water and Methanol Ice in L 1544. *Astron. Astrophys.* **2021**, *651*, A53.

(3) Watanabe, N.; Kouchi, A. Efficient Formation of Formaldehyde and Methanol by the Addition of Hydrogen Atoms to CO in H2O-CO Ice at 10 K. *Astrophys. J.* **2002**, *571* (2), L173.

(4) Watanabe, N.; Nagaoka, A.; Hidaka, H.; Shiraki, T.; Chigai, T.; Kouchi, A. Dependence of the Effective Rate Constants for the Hydrogenation of CO on the Temperature and Composition of the Surface. *Planet. Space Sci.* **2006**, *54* (11), 1107−1114.

(5) Dias, N.; Lemmens, A. K.; Wannenmacher, A.; Ahmed, M. Vacuum Ultraviolet Photoionization of Methane-Water Clusters Leads to Methanol Formation. *ACS Earth Space Chem.* **2024**, *8*, 1867−1876.

(6) Basalgète, R.; Dupuy, R.; Féraud, G.; Romanzin, C.; Philippe, L.; Michaut, X.; Michoud, J.; Amiaud, L.; Lafosse, A.; Fillion, J. H.; Bertin, M. Complex Organic Molecules in Protoplanetary Disks: X-Ray Photodesorption from Methanol-Containing Ices - I. Pure Methanol Ices. *Astron. Astrophys.* **2021**, *647*, A35.

(7) Torres-Díaz, D.; Basalgète, R.; Bertin, M.; Fillion, J. H.; Michaut, X.; Amiaud, L.; Lafosse, A. Cryogenic Chemistry and Quantitative Non-Thermal Desorption from Pure Methanol Ices: High-Energy Electron versus X-Ray Induced Processes. *ChemPhysChem* **2023**, *24* (9), No. e202200912.

(8) Akerman, M. S.; Iny, H.; Sagi, R.; Asscher, M. Chemical Reactivity of Strongly Interacting, Hydrogen-Bond-Forming Molecules Following 193 Nm Photon Irradiation: Methanol in Amorphous Solid Water at Low Temperatures. *Langmuir* **2023**, *39* (7), 2838−2849.

(9) Schmidt, F.; Swiderek, P.; Bredehöft, J. H. Electron-Induced Processing of Methanol Ice. *ACS Earth Space Chem.* **2021**, *5* (2), 391−408.

(10) Whittet, D. C. B.; Cook, A. M.; Herbst, E.; Chiar, J. E.; Shenoy, S. S. Observational Constraints on Methanol Production in Interstellar and Preplanetary Ices. *Astrophys. J.* **2011**, *742* (1), 28.

(11) Sekine, Y.; Genda, H.; Muto, Y.; Sugita, S.; Kadono, T.; Matsui, T. Impact Chemistry of Methanol: Implications for Volatile Evolution on Icy Satellites and Dwarf Planets, and Cometary Delivery to the Moon. *Icarus* **2014**, *243*, 39−47.

(12) Malla, B. K.; Vishwakarma, G.; Chowdhury, S.; Selvarajan, P.; Pradeep, T. Formation of Ethane Clathrate Hydrate in Ultrahigh Vacuum by Thermal Annealing. *J. Phys. Chem. C* **2022**, *126* (42), 17983−17989.

(13) Chowdhury, S.; Malla, B. K.; Vishwakarma, G.; Nyayban, A.; Pradeep, T. Composition-Dependent Formation and Dissociation of Structure I and Structure II Clathrate Hydrates of Trimethylene Oxide in Ultrahigh Vacuum. *J. Phys. Chem. C* **2025**, *129* (19), 8937−8945.

(14) Vishwakarma, G.; Malla, B. K.; Chowdhury, S.; Khandare, S. P.; Pradeep, T. Existence of Acetaldehyde Clathrate Hydrate and Its Dissociation Leading to Cubic Ice under Ultrahigh Vacuum and Cryogenic Conditions. *J. Phys. Chem. Lett.* **2023**, *14* (23), 5328−5334.

(15) Malla, B. K.; Vishwakarma, G.; Chowdhury, S.; Nayak, S. K.; Yamijala, S. S. R. K. C.; Pradeep, T. Formation and Dissociation of Dimethyl Ether Clathrate Hydrate in Interstellar Ice Mimics. *J. Phys. Chem. C* **2024**, *128* (6), 2463−2470.
(16) Malla, B. K.; Yang, D.-S.; Pradeep, T. Growth of Clathrate Hydrates in Nanoscale Ice Films Observed Using Electron Diffraction and Infrared Spectroscopy. *J. Phys. Chem. Lett.* **2025**, *16*, 365−371.
(17) Malla, B. K.; Chowdhury, S.; Bhardwaj, K.; Kumar, R.; Pradeep, T. Water Cages as Chemical Reactors: VUV Photolysis of Dimethyl Ether Clathrate Hydrate Thin Films in Ultrahigh Vacuum. *J. Phys. Chem. Lett.* **2026**, *17* (12), 3662−3669.
(18) Vishwakarma, G.; Malla, B. K.; Reddy, K. S. S. V. P.; Ghosh, J.; Chowdhury, S.; Yamijala, S. S. R. K. C.; Reddy, S. K.; Kumar, R.; Pradeep, T. Induced Migration of CO2 from Hydrate Cages to Amorphous Solid Water under Ultrahigh Vacuum and Cryogenic Conditions. *J. Phys. Chem. Lett.* **2023**, *14*, 2823−2829.
(19) Tychengulova, A.; Katpayeva, K.; Shomshekova, S.; Ibragimova, S.; Golikov, O.; Yerezhep, D.; Sokolov, D.; Aldiyarov, A. Laboratory Studies of the Clathrate Hydrate Formation in the Carbon Dioxide-Water Mixtures at Interstellar Conditions. *ACS Omega* **2025**, *10*, 1237.
(20) Shin, K.; Moudrakovski, I. L.; Ratcliffe, C. I.; Ripmeester, J. A. Managing Hydrogen Bonding in Clathrate Hydrates by Crystal Engineering. *Angew. Chem., Int. Ed.* **2017**, *56* (22), 6171−6175.
(21) Blake, D.; Allamandola, L.; Sandford, S.; Hudgins, D.; Freund, F. Clathrate Hydrate Formation in Amorphous Cometary Ice Analogs in Vacuo. *Science* **1991**, *254* (5031), 548−551.
(22) Williams, K. D.; Devlin, J. P. Formation and Spectra of Clathrate Hydrates of Methanol and Methanol-Ether Mixtures. *J. Mol. Struct.* **1997**, *416* (1−3), 277−286.
(23) Devlin, J. P. Catalytic Activity of Methanol in All-Vapor Subsecond Clathrate-Hydrate Formation. *J. Chem. Phys.* **2014**, *140* (16), No. 164505.
(24) Shin, K.; Udachin, K. A.; Moudrakovski, I. L.; Leek, D. M.; Alavi, S.; Ratcliffe, C. I.; Ripmeester, J. A. Methanol Incorporation in Clathrate Hydrates and the Implications for Oil and Gas Pipeline Flow Assurance and Icy Planetary Bodies. *Proc. Natl. Acad. Sci. U. S. A.* **2013**, *110* (21), 8437−8442.
(25) Bag, S.; Bhuin, R. G.; Methikkalam, R. R. J.; Pradeep, T.; Kephart, L.; Walker, J.; Kuchta, K.; Martin, D.; Wei, J. Development of Ultralow Energy (1−10 EV) Ion Scattering Spectrometry Coupled with Reflection Absorption Infrared Spectroscopy and Temperature Programmed Desorption for the Investigation of Molecular Solids. *Rev. Sci. Instrum.* **2014**, *85* (1), 014103.
(26) Schriver-Mazzuoli, L.; Coanga, J. M.; Schriver, A.; Ehrenfreund, P. Infrared Spectra of (CH3)2O and (CH3)2O + H2O at Low Temperature. *Vib. Spectrosc.* **2002**, *30* (2), 245−257.
(27) Hudson, R. L.; Gerakines, P. A.; Yarnall, Y. Y. Infrared Spectroscopic and Physical Properties of Methanol Ices—Reconciling the Conflicting Published Band Strengths of an Important Interstellar Solid. *Astrophys. J.* **2024**, *970* (2), 108.
(28) Gálvez, Ó.; Maté, B.; Martín-Llórente, B.; Herrero, V. J.; Escribano, R. Phases of Solid Methanol. *J. Phys. Chem. A* **2009**, *113* (14), 3321−3329.
(29) Dawes, A.; Mason, N. J.; Fraser, H. J. Using the C−O Stretch to Unravel the Nature of Hydrogen Bonding in Low-Temperature Solid Methanol−Water Condensates. *Phys. Chem. Chem. Phys.* **2016**, *18* (2), 1245−1257.
(30) Müller, B.; Giuliano, B. M.; Goto, M.; Caselli, P. Spectroscopic Measurements of CH3OH in Layered and Mixed Interstellar Ice Analogues. *Astron. Astrophys.* **2021**, *652*, A126.
(31) Su, Z.; Alavi, S.; Ripmeester, J. A.; Wolosh, G.; Dias, C. L. Methane Clathrate Formation Is Catalyzed and Kinetically Inhibited by the Same Molecule: Two Facets of Methanol. *J. Phys. Chem. B* **2021**, *125* (16), 4162−4168.
(32) Amtawong, J.; Guo, J.; Hale, J. S.; Sengupta, S.; Fleischer, E. B.; Martin, R. W.; Janda, K. C. Propane Clathrate Hydrate Formation Accelerated by Methanol. *J. Phys. Chem. Lett.* **2016**, *7* (13), 2346−2349.
(33) Lauricella, M.; Ghaani, M. R.; Nandi, P. K.; Meloni, S.; Kvamme, B.; English, N. J. Double Life of Methanol: Experimental Studies and Nonequilibrium Molecular-Dynamics Simulation of Methanol Effects on Methane-Hydrate Nucleation. *J. Phys. Chem. C* **2022**, *126* (13), 6075−6081.
(34) Abay, H. K.; Svartaas, T. M. Effect of Ultralow Concentration of Methanol on Methane Hydrate Formation. *Energy Fuels* **2010**, *24* (2), 752−757.
(35) Davidson, D. W.; Gough, S. R.; Ripmeester, J. A.; Nakayama, H. The Effect of Methanol on the Stability of Clathrate Hydrates. *Can. J. Chem.* **1981**, *59* (17), 2587−2590.
(36) Sloan, E. D., Jr.; Koh, C. A.; Koh, C. A. Clathrate Hydrates of Natural Gases. *Clathrate Hydrates of Natural Gases.* **2007**, DOI: 10.1201/9781420008494.
(37) Malla, B. K.; Chowdhury, S.; Nayak, S. K.; Baji, S. S.; Mathew, T. J.; Methikkalam, R. R. J.; Yamijala, S. S. R. K. C.; Kumar, R.; Pradeep, T. Secondary Guest-Driven Nucleation of N2O Clathrate Hydrate in Amorphous Ice Mixture under Ultrahigh Vacuum. *J. Phys. Chem. Lett.* **2025**, *16*, 12720−12727.
(38) Yee, N.; Chottiner, G. S.; Scherson, D. A. CO Adsorption on Ru-Modified Pt(100) Surfaces: Infrared Reflection Absorption Studies in Ultrahigh Vacuum. *J. Phys. Chem. B* **2004**, *108* (19), 5847−5850.
(39) Zaki, E.; Mirabella, F.; Ivars-Barceló, F.; Seifert, J.; Carey, S.; Shaikhutdinov, S.; Freund, H. J.; Li, X.; Paier, J.; Sauer, J. Water Adsorption on the Fe3O4(111) Surface: Dissociation and Network Formation. *Phys. Chem. Chem. Phys.* **2018**, *20* (23), 15764−15774.
(40) Smith, R. S.; Yuan, C.; Petrik, N. G.; Kimmel, G. A.; Kay, B. D. Crystallization Growth Rates and Front Propagation in Amorphous Solid Water Films. *J. Chem. Phys.* **2019**, *150* (21), No. 214703.
(41) Carrascosa, H.; Satorre, M. A.; Escribano, B.; Martín-Domenech, R.; Muñoz Caro, G. M. Physical Properties of Methanol (CH3OH) Ice as a Function of Temperature: Density, Infrared Band Strengths, and Crystallization. *Mon. Not. R. Astron. Soc.* **2023**, *525* (2), 2690−2700.

https://doi.org/10.1021/acs.jpclett.6c01720
J. Phys. Chem. Lett. XXXX, XXX, XXX−XXX